J Appl Electrochem (2014) 44:735–740
DOI 10.1007/s10800-014-0681-3

RESEARCH ARTICLE

Controllable growth of Bi_2O_3 with rod-like structures via the surfactants and its electrochemical properties

Hong Su · Shuiliang Cao · Nannan Xia · Xiangjin Huang · Jing Yan · Quanying Liang · Dingsheng Yuan

Received: 24 October 2013 / Accepted: 6 March 2014 / Published online: 19 March 2014

Abstract This paper reports a systematic study of the synthesis of rod-like Bi_2O_3 via a facile one-step precipitation method with the addition of different surfactants. The formation mechanisms for the surfactants assisted chemical precipitation method of rod-like Bi_2O_3 have been briefly discussed. The electrochemical measurement shows the Bi_2O_3 prepared by using P123 as surfactant exhibits the largest specific capacitance of 1,350 F g^{-1} at current density of 0.1 A g^{-1} as well as superior rate capability and excellent cycle stability. The scalable syntheses and prominent capacitive properties of this material suggest its potential applications in energy storage.

Keywords Rod-like Bi_2O_3 · Surfactants · Specific capacitance · Energy storage

1 Introduction

Stabilized bismuth oxides (Bi_2O_3) are important transition metal oxides, which have attracted great attention recently because of their wide band gap, high refractive index, dielectric permittivity and oxide ionic conductivity [1–3]. The Bi_2O_3 is a complex compound that has five main polymorphic forms, known as α, β, γ, δ, and ω-Bi_2O_3. Both of the low-temperature α and the high-temperature δ phases are stable, but the others are metastable phases [4–6]. Due to their unique physical properties and a variety of crystal morphologies, bismuth oxide is widely used in optical materials [4, 7], catalysts [8], electrolyte materials [9], gas sensors [10], and so on. Besides, nanocrystalline Bi_2O_3 can provide large surface area, electrochemical stability and pseudo-capacitive behavior, which is expected to make a significant contribution for the advancement of supercapacitors [11]. Up to now, there are only a few reports on the electrochemical properties of Bi_2O_3-based electrodes. For example, Gujar et al. [11] had firstly reported the Bi_2O_3 thin films as electrode material for supercapacitors, the specific capacitance of Bi_2O_3 thin films prepared by electrodeposition was only 98 F g^{-1}, but they displayed high electrochemical reversibility. Tong's group [12] had prepared novel hierarchical rippled Bi_2O_3 nanobelts with a high specific capacitance of 250 F g^{-1} and good electrochemical stability by an electrodeposition route. Wang and coworkers [13] had developed a facile solvothermal method for preparing the graphene nanosheet–bismuth oxide composite, which exhibited remarkable rate capability and well reversibility. Meanwhile, the specific capacitance of bismuth oxide was up to 757 F g^{-1} even at a high current density of 10 A g^{-1}. Yuan's group [14, 15] had successfully prepared mesoporous carbon@Bi_2O_3 composites by simple precipitation method and quick microwave method method. Due to producing the pseudo-capacitance from Bi_2O_3, the specific capacitances of the carbon-based composites were further improved than the pure porous carbon.

Various strategies have been used to synthesize different shapes of bismuth oxide, such as chemical vapor deposition

H. Su
Institute of Hydrobiology, Engineering Research Center of Tropical and Subtropical Aquatic Ecological Engineering, Ministry of Education, Jinan University, Guangzhou 510632, People's Republic of China

S. Cao
Center of Analysis and Testing, Jinan University, Guangzhou 510632, People's Republic of China

N. Xia · X. Huang · J. Yan · Q. Liang · D. Yuan (✉)
Department of Chemistry, Jinan University, Guangzhou 510632, People's Republic of China
e-mail: tydsh@jnu.edu.cn

[2, 16], electrodeposition [11, 12], atomic layer deposition [17], chemical precipitation methods [1, 18], etc. Among them, the chemical precipitation is believed to be the most convenient and practical one, due to it not only can avoid complicated processes but also be used for large-scale synthesis. In this work, we synthesized a series of rod-like Bi_2O_3 materials using $Bi(NO_3)_3$ as the Bi source, NaOH as precipitant and different surfactants as template by a direct precipitation method. The Bi_2O_3 crystals with controllable morphology can be obtained through this surfactant-assisted chemical precipitation method. Furthermore, the formation mechanisms and the electrochemical properties of the obtained Bi_2O_3 were discussed and presented.

2 Materials and methods

2.1 Sample synthesis

Polyethylene glycol 400(PEG-400), poly(ethylene oxide)-*block*-poly(propylene oxide)-*block*-poly(ethylene oxide) copolymer $EO_{20}PO_{68}EO_{20}$ (P123), hexadecyl trimethyl ammonium bromide (CTAB), and sodium dodecyl sulfate (SDS) were purchased from Sigma-Aldrich Co. Ltd. The other chemical reagents were obtained from different Chemical Reagent Co. Ltd. in China. All the reagents were used without further purification. 20 mL PEG-400 30 mL H_2O was added into $Bi(NO_3)_3$ of 0.05 mol L^{-1} solution under stirring at room temperature. Then, the 0.1 mol L^{-1} NaOH solution was added to the above solution under stirring at 65 °C for 2 h. After that, the mixture was diluted to 200 mL. The pale yellow precipitate was collected by centrifugation after washing several times with deionized water and ethanol, and dried in air at 60 °C. The sample was labeled as B_{PEG}.

Hundred milligram P123, CTAB and SDS were dissolved in 20 mL ethanol, respectively. The mixture was stirred and aged after $Bi(NO_3)_3$ solution was added. Subsequently, the NaOH solution was added to the reaction system under vigorous stirring. The resulting samples were collected and washed with deionized water and ethanol for several times, and dried in air at 60 °C. The samples were labeled as B_{P123}, B_{CTAB}, and B_{SDS}, respectively.

2.2 Characterization

The structure of the samples was analyzed by a MSAL-XD2 X-ray diffractometer (Cu Kα, 36 kV, 20 mA, $\lambda = 1.5406$ Å). The morphologies were examined by a Philips SEM-XL30S scanning electron microscope and high-resolution transmission electron microscope (HRTEM, JEOL JEM-2100F).

2.3 Electrochemical measurements

The working electrode was prepared by mixing an active material (80 wt%) with carbon black (15 wt%) and PTFE (5 wt% W.M.: 4–5 × 10^6). The viscous slurry was painted onto two pieces of nickel form with an area of 1 cm^2 and pressed pressed under 25 MPa. The mass loading of the active material was about 8.0 mg cm^{-2} All electrochemical measurements were performed on a CHI660D electrochemical workstation with a potential range between −0.9 and 0.1 V. The experiments were carried out in a standard three electrodes cell containing a nickel foil as current collector. A Pt plate (1.0 cm × 1.0 cm) and an Hg/HgO electrode used as counter and reference electrode. The electrodes were measured by cyclic voltammetry (CV) and galvanostatic charge/discharge in a 6 M KOH aqueous solution.

3 Results and discussion

The XRD patterns of as-prepared Bi_2O_3 materials by applying four different surfactants are shown in Fig. 1. The sample B_{PEG} and B_{P123} prepared through using PEG-400 and P123 as surfactants present sharp and well-defined peaks, respectively. The main peaks for B_{PEG} and B_{P123} appear at $2\theta = 27.4°$, 33.3°, 46.4°, 52.4°, and 54.9°, corresponding to the monoclinic α-Bi_2O_3 with lattice constants $a = 5.83$ Å, $b = 8.14$ Å, and $c = 7.48$ Å (JCPDS: 76–1730), suggesting that both sample B_{PEG} and B_{P123} are α-Bi_2O_3 without impurity phases. The XRD pattern of sample B_{SDS} using SDS as structure directing agent is also well matched with pure monoclinic α-Bi_2O_3 (JCPDS 76-1730). And the sample

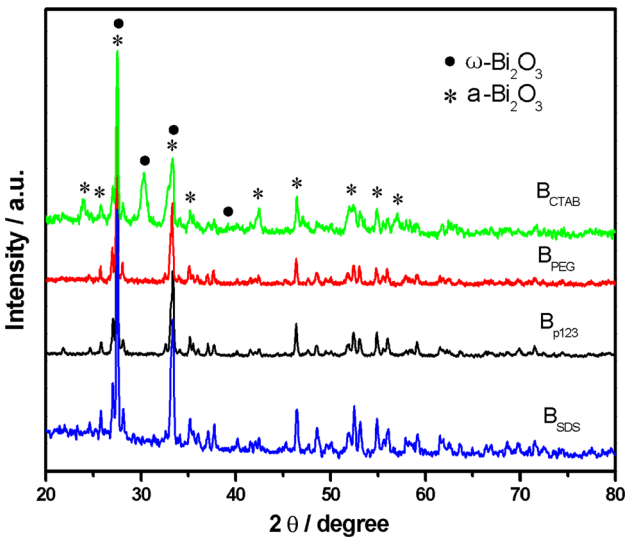

Fig. 1 XRD patterns of as-prepared B_{PEG}, B_{P123}, B_{CTAB} and B_{SDS}

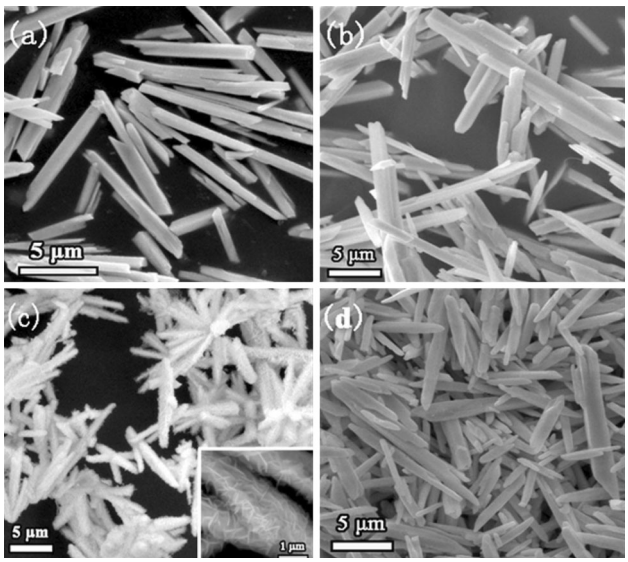

Fig. 2 SEM images of the as-synthesized Bi_2O_3 with different surfactants: **a** B_{PEG}, **b** B_{P123}, **c** B_{CTAB}, and **d** B_{SDS}

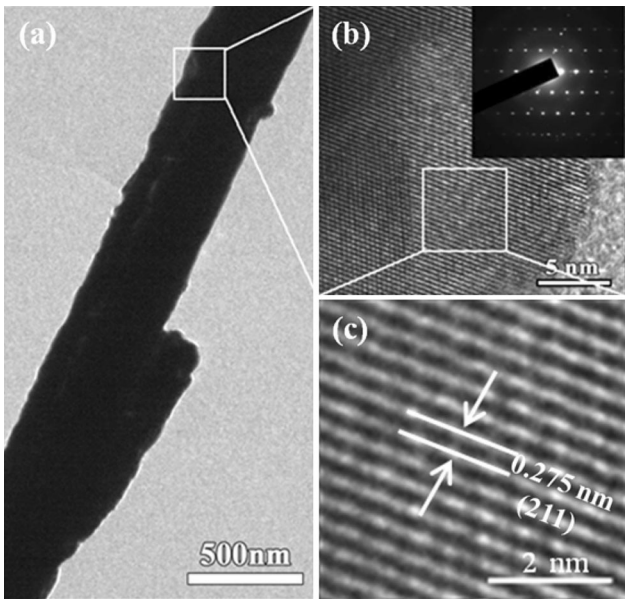

Fig. 3 **a** TEM and **b**, **c** HRTEM images and SEAD pattern (*inset*) of the B_{P123}

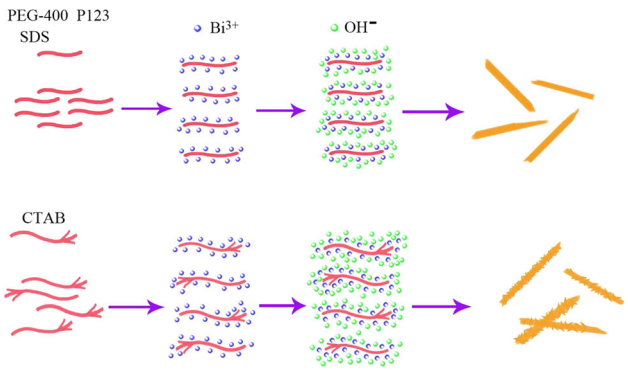

Fig. 4 Formation mechanisms of the rod-like Bi_2O_3

B_{CTAB} using CTAB as surfactant displays distinct peaks at $2\theta = 27.4°$, 30.2°, 33.3°, 42.4°, and 46.4°, which are consistent with the standard JCPDS 76–1730 and 50–1088 values, indicating that B_{CTAB} is composed of monoclinic α-Bi_2O_3 and anorthic ω-Bi_2O_3.

Figure 2 shows the SEM images of Bi_2O_3 samples synthesized with the aid of different surfactants. Fig. 2a presents the SEM image of sample B_{PEG}. It can be clearly seen that the as-synthesized Bi_2O_3 is smooth rods with non-agglomerated. The morphologies of sample B_{P123} (Fig. 2b) and B_{SDS} (Fig. 2d) obtained via direct precipitation method at room temperature show smooth rod-like shapes with different sizes in the presence of P123 and SDS, respectively. Remarkably, as shown in Fig. 2c, the sample B_{CTAB} synthesized with CTAB as surfactant gives the rod-like structures containing numerous nanosheets. The diameter and length of Bi_2O_3 nanorod are 400–450 nm and ~10 μm, respectively. A higher magnification SEM image (inset of Fig. 2c) reveals the nanosheet-stacking structures of Bi_2O_3.

The detailed crystal structure and composition of the product were further characterized using transmission electron microscopy (TEM). Fig. 3a, b is the TEM and HRTEM images and selected area electron diffraction pattern (SAED) of B_{P123}, which clearly shows the nanorod diameter is about 400 nm. An enlarged HRTEM image of the Bi_2O_3 nanorod recorded from the white square is presented in Fig. 3c. Such nanorod nanostructure exhibits a slightly larger Bi_2O_3 (211) plane spacing of 0.275 nm, and the SAED pattern in Fig. 3b from the as-prepared sample shows that the nanrod of Bi_2O_3 is of the single crystal structure.

Based on above-observed morphologies, the possible formation mechanism of the rod-like Bi_2O_3 is proposed in Fig. 4. First, the surfactant P123 as template was dispersed in aqueous solution. And then the Bi^{3+}-surfactant complex with high stability as the acidic solution containing Bi^{3+} was added to the solution, constant formed, which could change the rates of crystal nucleation and crystal growth. Secondly, when the NaOH solution was added to adjust the relatively high pH (≈13) with large amounts of Bi_2O_3 particles grew along the straight chains of P123 surfactants. Thus, the Bi_2O_3 nuclei grew and formed smooth Bi_2O_3 rods. Finally, the surfactant was removed from the unsubstantial point of Bi_2O_3 crystal by washing with deionized water and ethanol. However, when CTAB with branched chain structures was used as structure-directing

agent, the main of Bi_2O_3 particles grew along the main chains and formed rod-like structures, and other self-assembled into nanosheet Bi_2O_3 structures stacking on the Bi_2O_3 nanorods surfaces, which may be ascribed to the co-operation synergistic effects of Bi^{3+} and CTAB. Similarly, the surfactant was also removed from the unsubstantial point of Bi_2O_3 crystal by washing with deionized water and ethanol. For the deposition of Bi_2O_3 by chemical precipitation method in this process could be briefly described as follows [1]:

$$Bi^{3+} + 3OH^- \rightleftarrows Bi(OH)_3 \quad (1)$$

$$2Bi(OH)_3 \rightleftarrows Bi_2O_3 + 3H_2O \quad (2)$$

In order to evaluate the electrochemical characteristics of these rod-like Bi_2O_3 synthesized with different surfactants, CV and galvanostatic charge/discharge are employed to study the capacitance performance of the obtained Bi_2O_3. The CV curves of the Bi_2O_3 electrodes at the scan rate of 1 mV s^{-1} are presented in Fig. 5a. The shapes of the CV curves reveal that the capacitance feature is very distinguished from that of pure double-layer capacitor in which the shape is similar to an ideal rectangular shape, demonstrating that the total capacitance mainly results from the pseudo-capacitive capacitance. All the CV curves show a pair of distinct redox peaks, impling that these Bi_2O_3 between different valence states possess good redox transitions. When a potential difference is applied across the electrode in an alkaline solution, the redox reactions will occur and the charge will build up on the surface of electrode. Due to electrostatic interactions, ions in the solution, i.e., protons are transferred to the surface of the electrode to counterbalance the charge on the electrode during charge and discharge. Meanwhile, the electron transfer occurs through the current source or the external load. Therefore, the CV curves of the Bi_2O_3 electrodes are quite symmetrical. A probable redox mechanism for the formation of pseudo-capacitance of Bi_2O_3 in an alkaline solution is proposed according to the following reaction [19],

$$Bi_2O_3 + 3H_2O + 6e^- \underset{\text{discharge}}{\overset{\text{charge}}{\rightleftharpoons}} Bi + 6OH^- \quad (3)$$

Figure 5b shows the CV curves of B_{P123} electrode at different scan rates. The redox current intensities increase approximately proportionally with the increasing scan rates, indicating that electronic transfer process in the electrode and ionic diffusion in electrolyte are not the rate-limiting processes. It also should be found that positive shift of oxidation peaks and negative shift of reduction peaks with an increase of scan rate, it should be attributed to the reaction capability and the concentration of OH^- at the interface between electrode and electrolyte [20].

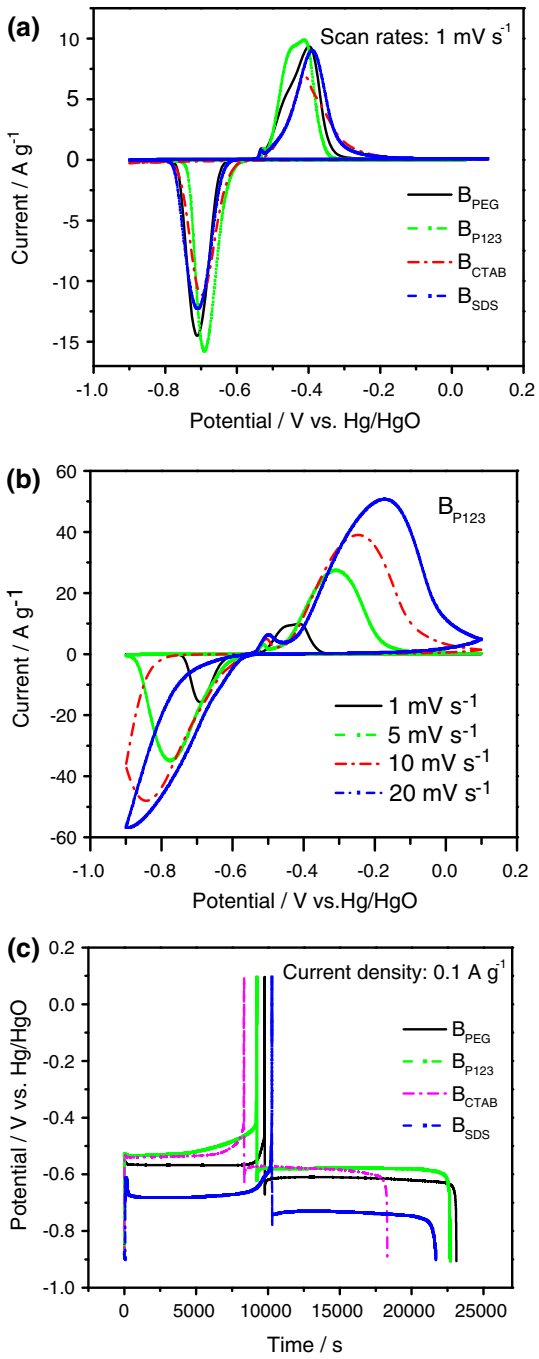

Fig. 5 **a** CV curves of the as-prepared Bi_2O_3 electrodes at the scan rate of 1 mV s^{-1}, **b** CV curves of B_{P123} electrode at different scan rates, and **c** galvanostatic charge/discharge curves of the as-prepared Bi_2O_3 electrodes at the current density of 0.1 A g^{-1}

The galvanostatic charge/discharge measurement is used to estimate the applicability for quick charge/discharge operation. Figure 5c displays the typical charge/discharge curves of the Bi_2O_3 electrodes at the current density of 0.1 A g^{-1}. The voltage–time curves also confirm the redox behaviors of the synthesized Bi_2O_3. The specific

capacitance of electrode is calculated from the discharge curve according to the following equation [21]:

$$C = \frac{it}{m\Delta V} \quad (4)$$

where i (A) is discharge current, t (s) denote the total discharge time, ΔV (V) is the total potential deviation of voltage window, and m (g) represents the mass of active materials in the electrode. The specific capacitances of the Bi_2O_3 electrodes with different current densities calculated from Eq. (4) are listed in Table 1. The discharge capacitances of the four Bi_2O_3 samples reach up to 1336, 1350, 996, and 1147 F g^{-1} at the current density of 0.1 A g^{-1}, and they decrease correspondingly to 920, 965, 892, and 880 F g^{-1} even at 2 A g^{-1}, suggesting that the Bi_2O_3 electrodes have superior charge/discharge properties at high current density. The specific capacitances reported herein are much larger than that 98 F g^{-1} of Bi_2O_3 thin films [11] and 250 F g^{-1} of hierarchical rippled Bi_2O_3 nanobelts [11]. This comparison illustrates a better utilization efficiency of the obtained rod-like Bi_2O_3. Thus, because of low cost, facile preparation, and excellent rate capabilities, the Bi_2O_3 electrodes are promise for fast and efficient energy storage.

The cycling stability of Bi_2O_3 prepared using P123 as structure directing agents is evaluated by repeated CV at a scan rate of 20 mV s^{-1}. As shown in Fig. 6, the specific capacitance of electrode drops from 632 to 617 F g^{-1}, losing only 2.4 % capacitance after 1,000 cycles, indicating that the Bi_2O_3 material as pseudo-capacitors electrode material has high electrochemical stability.

Table 1 Specific capacitance of as-synthesized Bi_2O_3 measured with galvanostatic charge/discharge in 6 M KOH aqueous solution

Sample name	Capacitance C (F g^{-1})				
	0.1 A g^{-1}	0.2 A g^{-1}	0.5 A g^{-1}	1 A g^{-1}	2 A g^{-1}
B_{PEG}	1,336	1,127	1,064	965	920
B_{P123}	1,350	1,128	1,080	1,066	965
B_{CTAB}	996	986	945	896	892
B_{SDS}	1,147	1,070	1,014	962	880

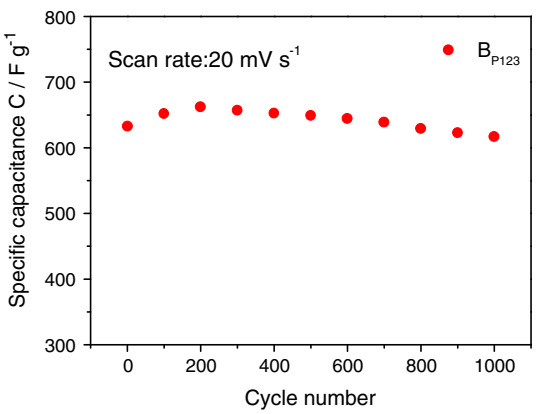

Fig. 6 Cycle-life performance of B_{P123} electrode

4 Conclusion

The rod-like Bi_2O_3 have been synthesized by employing cationic surfactant, anionic surfactant, and neutral surfactant as structure-directing agent. The surfactants with different chain structures can effectively affect the morphologies of the products. Moreover, this surfactant-assisted route may be extended to the preparation of rod-like structures of other compounds. Electrochemical studies show that the rod-like Bi_2O_3 using P123 as surfactant presents a maximum specific capacitance of 1,350 F g^{-1} at current density of 0.1 A g^{-1}, superior rate capability (71.4 % capacitance retention from 0.1 to 2 A g^{-1}), and excellent cycle stability (only 2.4 % capacitance decline after 1,000 cycles), suggesting that it is a promising electrode material for low-cost, high-performance supercapacitors application.

Acknowledgments The authors wish to acknowledge financial support from the National Natural Science Foundation of China (21031001 and 21376105) and 44th Scientific Research Foundation for the Returned Overseas Chinese Scholars, State Education Ministry.

References

1. Gujar TP, Shinde VR, Lokhande CD, Mane RS, Han SH (2005) Bismuth oxide thin films prepared by chemical bath deposition (CBD) method: annealing effect. Appl Surf Sci 250:161–167
2. Takeyama T, Takahashi N, Nakamura T, Itoh S (2005) Microstructure characterization of δ-Bi_2O_3 thin film under atmospheric pressure by means of halide CVD on c-sapphire. J Cryst Growth 275:460–466
3. Sammes NM, Tompsett GA, Nafë H, Aldinger F (1999) Bismuth based oxide electrolytes- structure and ionic conductivity. J Eur Ceram Soc 19:1801–1826
4. Fan HT, Teng XM, Pan SS, Ye C, Li GH, Zhang LD (2005) Optical properties ofδ-Bi_2O_3 thin films grown by reactive sputtering. Appl Phys Lett 87:231916
5. He WD, Qin W, Wu XH, Ding XB, Chen L, Jiang ZH (2007) The photocatalytic properties of bismuth oxide films prepared through the sol-gel method. Thin Solid Films 515:5362–5365
6. Ng SN, Tan YP, Taufiq-Yap YH (2009) Mechanochemical synthesis and characterisation of bismuth-niobium oxide ion conductors. J Phys Sci 20(1):75–86
7. Oprea II, Hesse H, Betzler K (2004) Optical properties of bismuth borate glasses. Opt Mater 26:235–237
8. Hanna TA (2004) The role of bismuth in the SOHIO process. Coord Chem Rev 248:429–440
9. Azad AM, Larose S, Akbar SA (1994) Bismuth oxide-based solid electrolytes for fuel cells. J Mater Sci 29:4135–4151
10. Adamian ZN, Abovian HV, Aroutiounian VM (1996) Smoke sensor on the base of Bi_2O_3 sesquioxide. Sens Actuators B 35:241–243

11. Gujar TP, Shinde VR, Lokhande CD, Han SH (2006) Electrosynthesis of Bi_2O_3 thin films and their use in electrochemical supercapacitors. J Power Sources 161:1479–1485
12. Zheng FL, Li GR, Ou YN, Wang ZL, Su CY, Tong YX (2010) Synthesis of hierarchical rippled Bi_2O_3 nanobelts for supercapacitor applications. Chem Commun 46:5021–5023
13. Wang HW, Hu ZA, Chang YQ, Chen YL, Lei ZQ, Zhang ZY, Yang YY (2010) Facile solvothermal synthesis of a graphene nanosheet-bismuth oxide composite and its electrochemical characteristics. Electrochim Acta 55:8974–8980
14. Yuan DS, Zeng JH, Kristian N, Wang Y, Wang X (2009) Bi_2O_3 deposited on highly ordered mesoporous carbon for supercapacitors. Electrochem Commun 11:313–317
15. Xia NN, Yuan DS, Zhou TX, Chen JX, Mo SS, Liu YL (2011) Microwave synthesis and electrochemical characterization of mesoporous carbon@Bi_2O_3 composites. Mater Res Bull 46:687–691
16. Shen XP, Wu SK, Zhao H, Liu Q (2007) Synthesis of single-crystalline Bi_2O_3 nanowires by atmospheric pressure chemical vapor deposition approach. Phys E 39:133–136
17. Shen YD, Li YW, Li WM, Zhang JZ, Hu ZG, Chu JH (2012) Growth of Bi_2O_3 ultrathin films by atomic layer deposition. J Phys Chem C 116:3449–3456
18. Li W (2006) Facile synthesis of monodisperse Bi_2O_3 nanoparticles. Mater Chem Phys 99:174–180
19. Bodé M, Cachet C, Bach S, Pereira-Ramos JP, Ginoux JC, Yu LT (1997) Rechargeability of MnO_2 in KOH media produced by decomposition of dissolved $KMnO_4$ and $Bi(NO_3)_3$ mixtures, Mn-Bi complexes. J Electrochem Soc 144:792–801
20. Li JT, Zhao W, Huang FQ, Manivannan A, Wu NQ (2011) Single-crystalline $Ni(OH)_2$ and NiO nanoplatelet arrays as supercapacitor electrodes. Nanoscale 3:5103–5109
21. Zang JF, Li XD (2011) In situ synthesis of ultrafine β-MnO_2/polypyrrole nanorod composites for high-performance supercapacitors. J Mater Chem 21:10965–10969